clinical bioenergetics

MDPI

Article

PLGA-Encapsulated Mitochondrial Hydrogen Sulphide Donor, AP39, Resolve Endothelial Inflammation via Mitochondria-Targeted Bioenergetic and Redox Modulation

Lissette Sanchez-Aranguren [1,2,*], Bahareh Hassanzadeh Moghadam [1], Mohamad Anas Al Tahan [1], Kacper Kruszyna [3], Jacob Baxandall [4], Hala Shokr [5] and Mandeep Kaur Marwah [1,2]

[1] Aston Medical School, College of Health and Life Sciences, Aston University, Birmingham B4 7ET, UK; m.altahan1@aston.ac.uk (M.A.A.T.); m.marwah1@aston.ac.uk (M.K.M.)
[2] Aston Research Centre for Health in Ageing (ARCHA), Aston University, Birmingham B4 7ET, UK
[3] Faculty of Pharmacy and Pharmacology, Department of Life Sciences, University of Bath, Bath BA2 7AY, UK
[4] Faculty of Natural Sciences, Department of Life Sciences, University of Bath, Bath BA2 7AY, UK
[5] Pharmacy Division, School of Health Sciences, Faculty of Biology, Medicine and Health, University of Manchester, Manchester M13 9PL, UK; hala.shokr@manchester.ac.uk
* Correspondence: l.sanchez-aranguren2@aston.ac.uk

Abstract

Vascular inflammation and endothelial dysfunction are key drivers in the development of cardiovascular and neurovascular diseases. Mitochondrial dysfunction and oxidative stress further amplify inflammatory cascades, emphasising the need for targeted strategies that restore endothelial homeostasis at the subcellular level. Hydrogen sulphide (H_2S) donors, such as AP39, offer cytoprotective benefits but are limited by short half-life and rapid release of the active compound, H_2S. We developed poly(lactic-co-glycolic acid) (PLGA) nanoparticles encapsulating AP39 (PLGA-AP39) to achieve sustained, mitochondria-targeted H_2S delivery. Nanoparticles were characterised by size, polydispersity, zeta potential, encapsulation efficiency, and in vitro release kinetics. Human umbilical vein endothelial cells (HUVEC) were exposed to TNF-α to induce inflammation, followed by treatment with free AP39 or PLGA-AP39. Anti-inflammatory effects were assessed by measuring IL-6, IL-8, and TGF-β levels. Mitochondrial function was evaluated using a Seahorse XFe24 Analyser, membrane potential assays, and mitochondrial ROS detection. Moreover, we investigated vascular function by analysing capillary-like tube formation and wound closure in response to treatments. PLGA-AP39 nanoparticles displayed a uniform size (~227 nm), low PDI, and high encapsulation efficiency (>78%). Sustained AP39 release was observed over seven days. Treatment with PLGA-AP39 significantly restored TNF-α-induced endothelial dysfunction and reduced TNF-α-induced release of IL-6, IL-8, and TGF-β compared to untreated controls. Seahorse analysis revealed restoration of maximal respiration and increased spare respiratory capacity. Encapsulated AP39 also preserved mitochondrial membrane potential and reduced mitochondrial ROS production, demonstrating enhanced protection against inflammation-induced metabolic dysfunction. This work establishes a novel nanoparticle-based strategy for prolonged, mitochondria-specific H_2S delivery to counteract vascular inflammation and enhance endothelial bioenergetics. The results from this work are pioneering in the generation of a novel delivery method for H_2S donors employing PLGA and represent a promising therapeutic avenue for treating chronic vascular inflammatory disorders.

Keywords: PLGA nanoparticles; AP39; hydrogen sulphide donor; endothelial inflammation; mitochondrial bioenergetics; TNF-α

Academic Editors: Sergej M. Ostojic, John T. Hancock, Jiankang Liu and Juan de Dios Alché Ramírez

Received: 21 October 2025
Revised: 26 January 2026
Accepted: 12 February 2026
Published: 14 February 2026

1. Introduction

Vascular inflammation and endothelial dysfunction are central processes in the pathophysiology of numerous diseases, including atherosclerosis, stroke, and neurodegeneration [1–3]. In these conditions, the endothelium, a monolayer of cells lining the blood vessels, becomes compromised, leading to heightened permeability, leukocyte adhesion, and the perpetuation of inflammatory responses [4]. This cascade of events is further exacerbated by the increased generation of reactive oxygen species (ROS), which plays a critical role in damaging endothelial cells, ultimately contributing to the onset and progression of these diseases [1,5]. Central to this pathological loop is the role of mitochondria, both as source and target of ROS [6,7]. Mitochondrial dysfunction amplifies imbalance in ROS, leading to oxidative stress, reduces ATP generation, and disrupts redox signalling, thus accelerating endothelial injury [1–3].

Hydrogen sulphide (H_2S) is increasingly recognised as a potent cytoprotective gasotransmitter with significant implications for vascular health. H_2S acts as a signalling molecule, influencing cellular processes such as vasodilation, apoptosis, ROS quenching and inflammation [8–10]. In particular, mitochondria-targeted H_2S donors, such as AP39, have shown promise in this regard, as they can deliver H_2S directly to the mitochondria [11], thus amplifying its therapeutic antioxidant effects while minimising systemic side effects [12–15]. By delivering H_2S directly to the mitochondria, AP39 engages with intracellular targets (mitochondria) with high specificity, leading to enhanced mitochondrial efficiency, reduced oxidative damage, and improved endothelial function [12,15]. Mechanistic studies have highlighted its role in activating pathways such as PI3K/Akt/eNOS [16], which further augment nitric oxide (NO) bioavailability, a critical mediator of vascular health [17]. Other mechanistic studies have shown an anti-inflammatory role for H_2S donors, including their mediated roles in Nrf2 antioxidant response [18], S-sulfhydration of endothelial nitric oxide synthase (eNOS) [16], and NF-κB inhibition [19]. Despite these promising attributes, the clinical translation of H_2S-based therapies is constrained by the molecule's inherent volatility and rapid release of the active compound, H_2S [20]. This pharmacokinetic liability necessitates delivery strategies capable of preserving its bioactivity while enabling sustained and localised release.

Poly(lactic-co-glycolic acid) (PLGA) polymeric nanoparticles offer a compelling solution to this challenge [21]. PLGA is an FDA-approved biodegradable and biocompatible polymer offering controlled release properties. These features make PLGA-based delivery systems an attractive approach for targeted delivery of small molecules and biologics [21]. When adapted for intracellular delivery, such systems can facilitate cytosolic and organelle-level access to therapeutic payloads. Palma-Chavez et al. (2021) previously developed a PLGA-based delivery system where they observed that this delivery method improved the delivery of nanoparticles (NPs) targeting the endothelium [22]. The use of PLGA to deliver gaseous donors such as H_2S releasing compounds is novel. However, our previous work has successfully proven PLGA as a suitable carrier for sodium thiosulphate [23]. In this work, we first reported an optimised method for PLGA preparation suitable for H_2S donors' delivery. Moreover, we showed that PLGA slows the release of H_2S from sodium thiosulphate while retaining sodium thiosulphate's pro-angiogenic properties [23].

The integration of PLGA-based delivery with mitochondrial-targeted signalling represents an underexplored yet highly strategic approach to modulating endothelial inflammation. In this study, we engineered and characterised PLGA NPs encapsulating AP39 and evaluated their ability to modulate inflammatory responses in human endothelial cells exposed to TNF-α. Here, we report a detailed nanoparticle physicochemical profiling, in vitro AP39 release kinetics, and functional assays assessing cytokine secretion, mitochondrial respiration, membrane potential, and ROS production. Using a combination of

drug delivery technologies (PLGA) with mitochondrial redox modulation strategy (AP39), this work establishes a new platform for sustained intracellular delivery of H_2S donors with spatial precision and mechanistic relevance, laying the groundwork for future clinical applications of H_2S therapies in vascular health.

2. Materials and Methods

2.1. Reagents

Poly(lactic-co-glycolic acid) (PLGA) mol wt 30,000–60,000 was obtained from Sigma-Aldrich, Dorset, England. TNF-α (#210-TA-005, R&D Systems, Oxford, UK) was dissolved in PBS with 0.1% BSA. AP39 is a mitochondrial targeted hydrogen sulphide donor consisting of the mitochondria targeting triphenylphosphonium (TPP+) group ester-linked with the H_2S donor ADTOH (5-(4-hydroxyphenyl)-3H-1,2- dithiole-3-thione) by a ten-carbon alkyl chain [14,24]. AP39 was obtained from Cayman Chemicals, Cambridge, UK.

2.2. Preparation of AP39-Loaded PLGA Nanoparticles (PLGA-AP39)

AP39-loaded poly(lactic-co-glycolic acid) (PLGA) nanoparticles (NPs) were prepared using a single emulsion solvent evaporation method, using our previously described methods [23]. In brief, PLGA (50:50 lactide:glycolide, 50 mg/mL) was dissolved in dichloromethane (DCM) over a period of four hours. To initiate emulsion formation (water-in-oil, W/O), 3 µL of AP39 (1 mg/mL in ethanol) was added dropwise to the DCM solution, alongside 1 mL of 5% (*w*/*v*) polyvinyl alcohol (PVA, aqueous). The mixture was subjected to ultrasonic agitation using an MSE Soniprep 150 Plus Ultrasonic Disintegrator (MSE Centrifuges Ltd, Heathfield, East Sussex, UK) (exponential probe tip) at an amplitude of 16 for 30 s, incorporating 5 s pauses every 10 s to prevent overheating.

Following emulsion formation, the dispersion was stirred overnight in 10 mL of 0.7% (*w*/*v*) aqueous PVA to facilitate solvent evaporation. NPs were subsequently isolated by centrifugation at 9500 RPM for 10 min (Labnet International, Prism™ R, Labnet International Inc., Edison, NJ, USA) and washed thoroughly with cold water to remove unencapsulated AP39 and residual PVA. The resulting nanoparticle pellet was resuspended in 5% (*w*/*v*) aqueous trehalose, flash-frozen in liquid nitrogen for 1–2 min, and lyophilised overnight using an Edwards Vacuum Modulyo Freeze Dryer (Edwards Vacuum, Burgess Hill, UK). Lyophilised samples were stored at –20 °C until further analysis (Figure 1A).

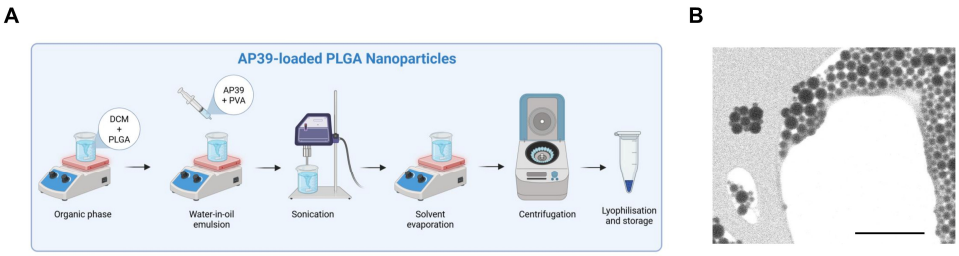

Figure 1. AP39-loaded PLGA nanofabrication and visualisation. (**A**) Schematic visualisation of the PLGA-NP fabrication method employing the single emulsion solvent evaporation technique. (**B**) Representative image of PLGA-NPs visualised using STEM, scale bar: 2 µm.

2.3. Characterisation of PLGA Nanoparticles Encapsulating AP39

Characterisation of the NPs, including determination of mean particle size, polydispersity index (PDI), and zeta potential, was conducted using standard protocols established within our laboratory [23]. Encapsulation efficiency was quantified by dissolving 2 mg of nanoparticles in 0.1 mL of acetonitrile, followed by centrifugation; the supernatant was analysed using high-performance liquid chromatography with ultraviolet detection (HPLC-UV) as we established previously in our laboratory [23].

Morphological characterisation of the PLGA NPs was performed using scanning transmission electron microscopy (STEM) under environmental scanning electron microscopy (ESEM) mode on a ThermoFisher Scientific Quattro S microscope (Waltham, MA, USA) equipped with a field emission filament. A drop of nanoparticle suspension (40 μg/mL) was placed onto a 200-mesh copper grid coated with holey carbon film. Imaging was carried out using the STEM3+ detector in Bright Field mode, with an acceleration voltage of 20–30 kV, a spot size between 2 and 4, and a variable pressure setting between 200 and 750 Pa to minimise beam damage. A representative image was obtained with a scale bar of 2 μm.

2.4. In Vitro Release Study of AP39 from PLGA-AP39

The release profile of AP39 from PLGA NPs was assessed in phosphate-buffered saline (PBS, pH 7.4) at 37 °C to simulate physiological conditions. Briefly, 10 mg of lyophilised PLGA-AP39 were reconstituted in 4 mL of PBS and incubated under gentle agitation. At predetermined time points (0, 2, 24, 48, and 120 h), 0.5 mL aliquots of the release medium were withdrawn and immediately replaced with an equal volume of fresh PBS to maintain sink conditions. Samples were centrifuged to remove residual NPs, and the supernatant was analysed by HPLC-UV to quantify the amount of AP39 released using protocols established in our lab [23].

2.5. H_2S Release from AP39

Free H_2S, a strong reducing agent, reacts with the tetrazolium dye 3-(4,5-dimethyl-2-thiazolyl)-2,5-diphenyl-2H-tetrazolium bromide (MTT, Sigma, St. Louis, MO, USA), resulting in the formation of a purple formazan product [23]. To assess H_2S release, HUVEC were exposed to either formulated PLGA-AP39 or AP39 in solution (0.2 μg/mL). After the designated exposure times, 100 μL of cell culture media was removed and combined with 100 μL of MTT (5 mg/mL) for a 3 h incubation. The reaction was conducted in a humidified incubator at 37 °C with a 5% CO_2 atmosphere to replicate cell culture conditions and prevent evaporation. Absorbance changes were measured up to 24 h using a plate reader at 570 nm. A H_2S calibration curve was generated by preparing serial dilutions of freshly dissolved sodium sulphide (Na_2S). H_2S generation was determined by measuring the hourly change in absorbance and correlating it to the respective H_2S concentrations.

2.6. Endothelial Cell Inflammation Model and Treatment

Human umbilical vein endothelial cells (HUVECs) were cultured in Endothelial Cell Growth Medium-2 (EGM-2, Promocell, Heidelberg, Germany) supplemented with 10% foetal bovine serum (FBS) and 1% penicillin/streptomycin and maintained at 37 °C in a humidified incubator with 5% CO_2.

To induce inflammation, HUVEC were exposed to TNF-α (10 ng/mL) for 24 h. Briefly, HUVEC were seeded in 24-well plates at 5×10^4 cells/well and allowed to reach 80–90% confluency prior to treatment with TNF-α. After 24 h, supernatant was collected to assess IL-6, IL-8 and TGF-β and confirm inflammation. To assess the effects of AP39 on inflammation, HUVEC exposed to TNF-α were co-treated with PLGA-AP39 NPs diluted in media for 24 h. In order to achieve a final concentration of AP39 of 0.3 μM, first, PLGA-AP39 NPs were prepared at a concentration of 5.6 μg/mL of AP39. Next, AP39-PLGA NPs were subsequently diluted in cell culture media as previously reported in our lab [12]. After 24 h co-treatment, supernatants were collected for cytokine release analysis.

2.7. Cytokine Release

We evaluated IL-6, IL-8 and TGF-β release using commercially available cytokine detection kits (IL-6: Human IL-6 DuoSet ELISA Catalog #: DY206; IL-8: Human IL-8/CXCL8 DuoSet ELISA Catalog #: DY208; TGF-β: Human TGF-beta 1 DuoSet ELISA

Catalog #: DY240), obtained from R&D Systems, Oxford, UK. Briefly, HUVEC were exposed to TNF-α and co-treated with PLGA-AP39 and respective controls. Cell media supernatant was collected after 24 h and stored at −20 °C until ELISA assessments were performed, following the manufacturer's instructions.

2.8. Tube Formation Assay

To assess the pro-angiogenic potential of PLGA-AP39, HUVEC were suspended in standard EGM-2 and plated in growth factor reduced Matrigel (Corning, Flintshire, UK) -coated 96-well plates at a density of 1×10^4 cells/well and let attach for 1 h at 37 °C in a humidified atmosphere of 5% CO_2. Following this, media was replaced with PLGA-AP39, TNF-α (10 ng/mL), or combination of these treatments, and dissolved in fresh DMEM containing 0.5% FBS for 4 h. After 4 h, cells were exposed to the fluorescent probe, calcein AM (1 μg/mL) for 20 min. Following, fluorescent images were taken using a Nikon TiE fluorescent inverted microscope (Ex/Em: 490/520 nm). The formation of capillary-like structures was quantified by measuring the total tube length, total branching length and total segment length using ImageJ (Fiji ImageJ, version 2.9.0) angiogenesis tool. Results are expressed in pixels.

2.9. Scratch Assay

Endothelial cell migration was assessed using a standard scratch wound healing assay. Briefly, HUVEC were seeded at a density of 5×10^4 cells/well in 24-well plates and let attach until reaching 100% confluence. Once a uniform monolayer was formed, cell cycles were synchronised by exposing cells to M199 media supplemented with 1% FBS for 1 h at 37 °C in a humidified atmosphere of 5% CO_2. Following, a straight scratch was created across the cell monolayer using a sterile 200 μL pipette tip. Detached cells were removed by washing twice with sterile PBS. Next, treatments were prepared in EGM-2 media. Cells were treated with TNF-α (10 ng/mL), PLGA-AP39 or combination of these treatments for 4 h and cells incubated under standard conditions (37 °C, 5% CO_2).

Wound closure was monitored by capturing phase-contrast images at 0 h and 4 h using an inverted microscope (×10 objective). The same wound area was imaged at each time point. The wound area was quantified using ImageJ software by measuring the distance between wound edges. Migration was expressed as the percentage of wound closure relative to the initial scratch area, calculated using the following equation:

$$Wound\ closure\ (\%) = \frac{(Initial\ wound\ area - Wound\ area\ at\ time\ X)}{Initial\ wound\ area} \times 100$$

2.10. Mitochondrial Bioenergetics

To evaluate the effects of AP39 delivered in PLGA-NP on TNF-α-mediated endothelial mitochondrial dysfunction, we utilised a Seahorse XFe24 Analyser (Agilent, Cheadle, Cheshire, UK) following protocols established in our lab [5,13,14]. Briefly, HUVEC were seeded onto V7 Seahorse 24-well plates at 3×10^4 cells/well and allowed to attach overnight at 37 °C in a humidified atmosphere of 5% CO_2. The following day, HUVEC were treated with TNF-α (10 ng/mL), or co-treated with TNF-α and PLGA-AP39 for 24 h and maintained at 37 °C in a humidified atmosphere of 5% CO_2. Following this, cells were washed, and media replaced with non-buffered DMEM (10 mM glucose, 1 mM pyruvate and 2 mM L-glutamine) to allow temperature and pH equilibrium. Subsequently, we evaluated oxygen consumption rates (OCR) in real-time using a Seahorse XFe24 Analyser (Agilent, Cheadle, Cheshire, UK). For this, we utilised the instrument built-in injection port functions to subsequently inject mitochondrial drugs/inhibitors: oligomycin (O) (1 μM) (Sigma Aldrich, Dorset, UK), carbonyl cyanide 4-(trifluoromethoxy) phenylhydrazone (FCCP) (0.5 μM) (Sigma Aldrich, Dorset, UK)

and a mixture of rotenone and antimycin A (A/R) (1 µM rotenone and 1 µM antimycin A, each applied at a final concentration of 1 µM in the assay) (Sigma Aldrich, Dorset, UK), which allowed to inhibit complex V (ATP-synthase), depolarise the mitochondrial membrane and inhibit complex I and III, respectively. As previously described [25], measurements of OCR following the injection of these drugs/inhibitors, allowed to calculate mitochondrial respiration parameters: basal and maximum respiration, spare respiratory capacity, ATP-linked respiration and non-mitochondrial respiration (Supplementary Figure S1). Data was expressed as the rate of OCR ($pmolO_2/min$) by time. OCR parameters were derived using the Seahorse XF Cell Mito Stress Test Report Generator (Agilent, Cheadle, Cheshire, UK) according to manufacturer guidelines. Non-mitochondrial respiration was defined as the minimum OCR measured following rotenone/antimycin A injection. Basal respiration was calculated as the last OCR measurement prior to the first injection minus non-mitochondrial respiration. Maximal respiration was calculated as the maximum OCR following FCCP injection minus non-mitochondrial respiration. Proton leak was defined as the minimum OCR following oligomycin injection minus non-mitochondrial respiration. ATP-linked respiration was calculated as the difference between the last OCR measurement before oligomycin injection and the minimum OCR after oligomycin injection. Spare respiratory capacity was calculated as the difference between maximal and basal respiration (Supplementary Figure S1).

2.11. Mitochondrial-Specific ROS

To confirm AP39 antioxidant properties to modulate mitochondrial-specific ROS, we employed the mitochondrial-specific probe MitoSOX Red (Sigma Aldrich, Dorset, UK). Briefly, HUVEC were treated with TNF-α (10 ng/mL), or co-treated with TNF-α and PLGA-AP39 for 24 h. Following, cells were exposed to 5 µM MitoSOX dissolved in PBS for 30 min at 37 °C in a humidified incubator with 5% CO_2 protected from light. After, cells were washed with PBS three times and fluorescence intensity was measured using a Tecan microplate reader (Tecan Group Ltd., Männedorf, Switzerland) (Ex/Em:510/580 nm) as previously established [26]. Fluorescence intensity was normalised to control and expressed as fold-change relative to control.

2.12. Mitochondrial Membrane Potential

To evaluate changes in mitochondrial membrane potential (ΔΨm), we employed the fluorescent dye, TMRE (Tetramethylrhodamine ethyl ester) (ab113852-TMRE Mitochondrial Membrane Potential Assay Kit, Abcam, Cambridge, UK). Briefly, 5.0×10^4 cells/well were plated in 24-well plates and let attach overnight. Following, cells were exposed to TNF-α (10 ng/mL) or co-treated with TNF-α and PLGA-AP39. After treatment, cells were exposed to 1 µM TMRE for 30 min and incubated at 37 °C in a humidified incubator with 5% CO_2 protected from light. After, cells were washed with PBS three times, followed by images of fluorescence taken using a Nikon TiE inverted microscope (Nikon, Derby, UK). Fluorescence intensity was calculated using ImageJ and results expressed as percentage of control.

2.13. ATP Levels

ATP levels were determined using the commercially available ATP Determination Kit (Invitrogen, Carlsbad, CA, USA). Briefly, 1.0×10^4 cells/well were plated in 96-well plates and let attach overnight. Following, cells were exposed to TNF-α (10 ng/mL) or co-treated with TNF-α and PLGA-AP39. After treatment, cell supernatant was collected and processed as per manufacturer's protocol. Luminescence intensity was read using a Tecan microplate reader. Readings were expressed as percentage of control.

2.14. Statistical Analysis

All results are presented as mean ± standard deviation (SD). All experiments were performed by duplicate and three independent experiments were carried out for all studies. For comparisons between two groups, Student's *t*-test was used. For comparisons between three or more groups, one-way ANOVA was performed, followed by Tukey's multiple comparisons post hoc test to assess direct differences between individual groups. A value of $p \leq 0.05$ was considered statistically significant. All the calculations were carried out using Graphpad 10.0.2 (GraphPad Inc., La Jolla, CA, USA).

3. Results

3.1. Characterisation of PLGA-AP39

PLGA-NPs loaded with AP39 were successfully synthesised using a single emulsion solvent evaporation method (Figure 1A) [23]. Characterisation using dynamic light scattering (DLS) revealed that the PLGA-NPs had a mean particle size of 226.9 ± 6.0 nm with a narrow PDI of 0.195 ± 0.039, indicating a uniform particle distribution. The zeta potential was +7.0 ± 2.5 mV, suggesting moderate colloidal stability. The encapsulation efficiency of AP39 was measured at 78.2 ± 3.0%, confirming successful drug loading. These results showed desirable ranges for NPs-based drug delivery systems (Table 1). In order to provide visualisation, PLGA-NPs were imaged by STEM (Figure 1B). As it can be depicted in the image, PLGA-NPs displayed a spherical shape. Nonetheless, this representative image does not constitute a quantitative assessment of particle size heterogeneity.

Table 1. Physicochemical characterisation of PLGA-NPs loaded with AP39.

Parameter	Value (Mean ± SD)
Particle Size (nm)	226.9 ± 6.0
Polydispersity Index (PDI)	0.195 ± 0.039
Zeta Potential (mV)	+7.0 ± 2.5
Entrapment Efficiency (%)	78.2 ± 3.0

PLGA-NPs were synthesised using a single emulsion solvent evaporation technique. Particle size, polydispersity index (PDI), and zeta potential (ZP) were measured using dynamic light scattering (DLS). Entrapment efficiency was determined by HPLC-UV analysis following NPs dissolution in acetonitrile. Data are presented as mean ± SD (n = 3).

3.2. Controlled Release of AP39 from PLGA-AP39

Once we confirmed homogenous distribution and size of PLGA-NPs loaded with AP39 (Figure 1, Table 1), we evaluated AP39 release patterns from these NPs and compared these results against AP39 non-encapsulated (in solution). AP39 in solution and PLGA-AP39 were observed over a seven-day period. Following, AP39 levels were measured using our established HPLC/UV methods. The release profile of AP39 from PLGA-NPs demonstrated a sustained and gradual release. Particularly, at the 2 h time point, we observed that approximately 33.3 ± 2.3% of the encapsulated AP39 was released. This increased to 68.2 ± 5.0% by 24 h, indicating a relatively rapid initial release phase. Subsequently, we observed a slower release pattern, with 80.4 ± 2.5% and 89.4 ± 1.1% cumulative release observed at 48 and 120 h, respectively (Figure 2). In contrast, AP39 in solution displayed a much faster release pattern, with 95 ± 4.58% released at the 2 h time point, followed by cumulative release of over 95% over the seven-day period (Figure 2). This behaviour was significantly different to AP39 encapsulated into PLGA-NPs, confirming that AP39 in solution offers an immediate availability of the active compound, H_2S, whereas encapsulation into PLGA allows a slower, controlled and sustained release.

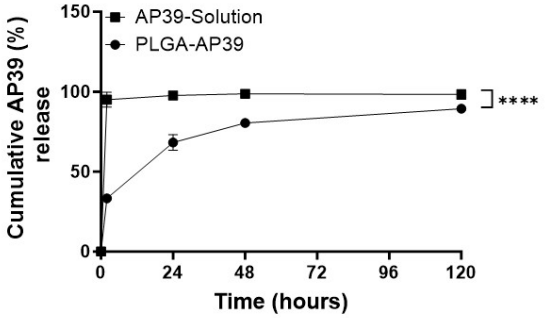

Figure 2. PLGA-NPs offer a sustained and controlled release of AP39. Cumulative AP39 release was determined over a seven-day period and AP39 levels determined by HPLC/UV methods. Data are presented as mean ± SD (n = 3), **** $p < 0.0001$.

3.3. H_2S Release from PLGA-AP39

Next, we examined the release kinetics of H_2S, the biologically active molecule in AP39, from both the AP39 in solution and PLGA-AP39 throughout a 48 h period. At the 1 h time point, both AP39 in solution as well as PLGA-AP39 displayed similar release kinetics of H_2S with AP39 in solution releasing 9.54 ± 2.05% of H_2S, while AP39-PLGA NPs released 7.19 ± 1.78%. At 2 h, AP39 in solution showed a maximum release of H_2S with 26.62 ± 3.22%, compared to 6.63 ± 2.16% for the PLGA-AP39 group (Figure 3). From the 3 h point measurement, it was observed that AP39 in solution released 14.77 ± 3.08% of H_2S. Subsequent time points showed the release continue to vary over time showing 13.72 ± 1.61% at 4 h and 11.77 ± 1.78% at 6 h. These values show that H_2S released from AP39 in solution have a maximum peak of release at approximately 2 h followed by a reduction in H_2S release leading to 6.57 ± 2.16% at 24 h and 7.43 ± 1.71% over 48 h.

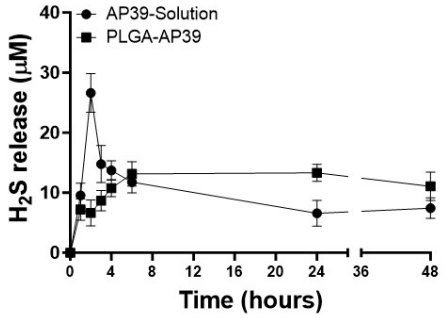

Figure 3. PLGA-AP39 provide a slower, more sustained release of H_2S. HUVEC were exposed to either AP39 in solution or PLGA-AP39. H_2S release was assessed over 48 h. Data represent the mean ± SD from three independent experiments (n = 3).

In contrast to these observations, when we evaluated H_2S release from PLGA-AP39, measured from the 3 h measurement point, we continued to observe a gradual and sustained increase of H_2S release exhibiting 8.68 ± 1.71% release at 3 h, followed by 10.75 ± 1.44% of H_2S at 4 h and 13.14 ± 2.04% at 6 h. At 24 h, PLGA-NPs encapsulating AP39 displayed the maximum release kinetics for H_2S observing 13.31 ± 1.43% H_2S release. By 48 h, PLGA-NPs released 11.05 ± 2.36% (Figure 3).

These results demonstrate that AP39 in solution releases the active molecule (H_2S) rapidly, displaying a "burst release" pattern whereas PLGA-AP39 provide a slower and more sustained release of H_2S. These results provide a significant advance in the translation of AP39 towards clinical use as these observations demonstrate that using PLGA-NPs allows sustained H_2S release and therefore ability to perform its biological actions offering an improved therapeutic window from administration to effect that extends from 2 h to 48 h.

3.4. PLGA-AP39 Reduces Vascular Inflammation

Once we confirmed that our approach of encapsulating AP39 into PLG-NPs provided a sustained release of AP39 and thus, H_2S, we investigated whether AP39 anti-inflammatory effects were retained while delivered in PLGA-NPs. HUVEC were exposed to TNF-α (10 ng/mL) to establish a pro-inflammatory environment. TNF-α was administered for 24 h at 10 ng/mL reflecting the existing literature supporting TNF-α-mediated Intercellular Adhesion Molecule 1, ICAM and E-selectin expression [27,28]. Moreover, cells were co-treated with PLGA-AP39. As observed in Figures 2 and 3, AP39 and thus H_2S released from PLGA provided a sustained and controlled release. The final concentration of AP39 administered to the cell culture was 0.3 μM. We aimed to observe whether this treatment with AP39 would resolve vascular inflammation by detecting cytokine release in cell supernatant.

We evaluated levels of IL-6, IL-8 and TGF-β using ELISA. As Figure 4 shows, TNF-α (10 ng/mL) induces a pro-inflammatory environment in HUVEC. Levels of IL-6 increased 2.8-fold (70.91 ± 3.7 pg/mL, $p < 0.0001$) when compared to control (25.83 ± 2.7 pg/mL). Moreover, when PLGA-AP39 were co-administered alongside TNF-α, we observed a significant reduction in IL-6 levels, to levels not statistically different to control (36.8 ± 2.9 pg/mL). When assessing IL-8 levels, we observed that TNF-α led to a significant increase in IL-8 levels (91.47 ± 8.4 pg/mL, compared to control, 37.42 ± 7.4 pg/mL, $p < 0.0001$) which were significantly reduced in the presence of AP39 encapsulated in PLGA-NPs (54.23 ± 7.4 pg/mL). Finally, we assessed levels of the pleiotropic cytokine, TGF-β. In the presence of TNF-α, TGF-β levels significantly increased (309 ± 21.38 pg/mL, $p < 0.0001$) compared to control (104.3 ± 5.1 pg/mL). Similar to our observations with IL-6 and IL-8, in the presence of AP39 encapsulated in PLGA-NPs, TGF-β levels significantly reduced to 191 ± 12.66 pg/mL. We explored the effects of TNF-α and AP39-PLGA NPs combined treatment on IL-10 levels (Supplementary Figure S2), and we did not observe changes induced by TNF-α alone, likely due to IL-10 being produced mainly by macrophages, dendritic cells and regulatory T cells [29]. These results suggest that AP39 counteract pro-inflammatory effects mediated by TNF-α when delivered in PLGA, supporting its delivery within this drug delivery system as a translational approach aiming to accelerate the use of AP39 as a therapeutic approach for diseases associated with vascular inflammation.

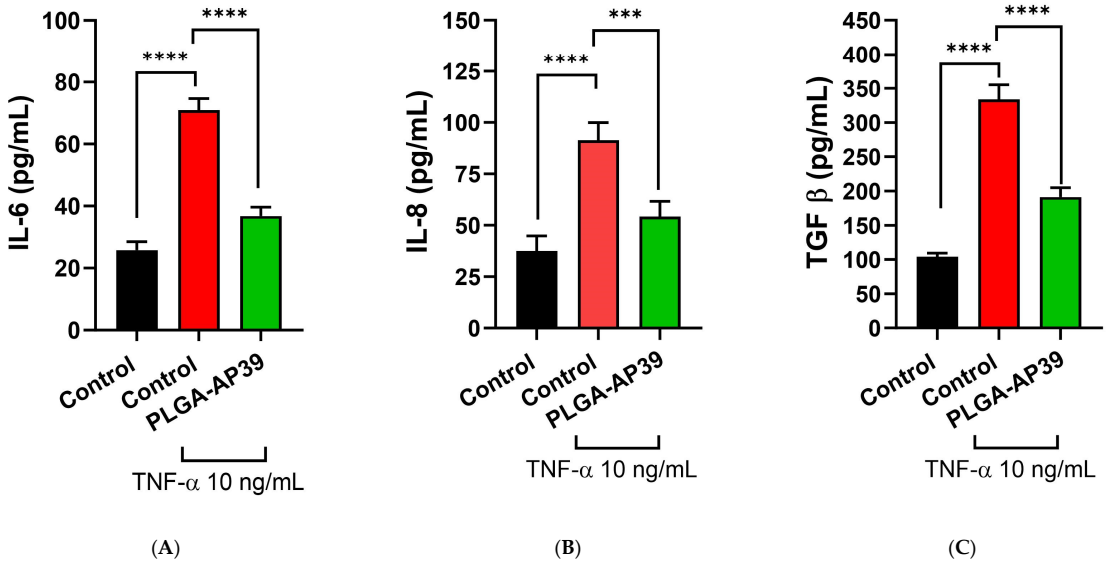

Figure 4. AP39 delivered in PLGA-NPs reduce vascular inflammation induced by TNF-α. (**A**) IL-6, (**B**) IL-8 and (**C**) TGF-β levels were detected in cell culture supernatant after exposure to TNF-α (10 ng/mL) or co-treated with TNF-α (10 ng/mL) and PLGA-AP39 diluted in media to final concentration of 0.3 μM. Data represent the mean ± SD from three independent experiments ($n = 3$), *** $p < 0.001$, **** $p < 0.0001$.

3.5. Mechanistic Insights into AP39-Mediated Modulation of Vascular Inflammation

AP39 has been increasingly recognised as an ROS quencher and modulator of cellular bioenergetics with improved roles within mitochondria, due to its intrinsic ability to accumulate within this organelle. To confirm whether AP39 delivered in PLGA-NPs was able to retain AP39 effects on mitochondrial bioenergetics, we used a Seahorse XFe24 Analyser to detect changes in OCR through time and calculate changes in the parameters of mitochondrial function (Supplementary Figure S1). Figure 5A shows traces of OCR by time measured in HUVEC exposed to TNF-α alone, PLGA-AP39 alone or TNF-α co-treated with PLGA-AP39. Figure 5B shows parameters of mitochondrial function calculated from Figure 5A. As depicted, treatments did not affect basal respiration or proton leak-linked OCR measurements. This is consistent with a pro-inflammatory environment where subtle changes in mitochondrial function can be observed before apoptosis is induced. We observed that TNF-α significantly reduced maximum respiration rates when compared to cells also treated with AP39 in PLGA-NPs ($p < 0.05$). Moreover, spare respiratory capacity was significantly reduced in the presence of TNF-α alone ($p < 0.01$). The combination of TNF-α and AP39 in PLGA-NPs yielded no statistical differences. Finally, we detected that both TNF-α and AP39 in PLGA-NPs provided a significant increase in ATP-linked OCR compared to control ($p < 0.05$), suggesting that AP39 promotes mitochondrial respiration coupled to ATP synthesis as an indicator of enhanced mitochondrial health (Figure 5B).

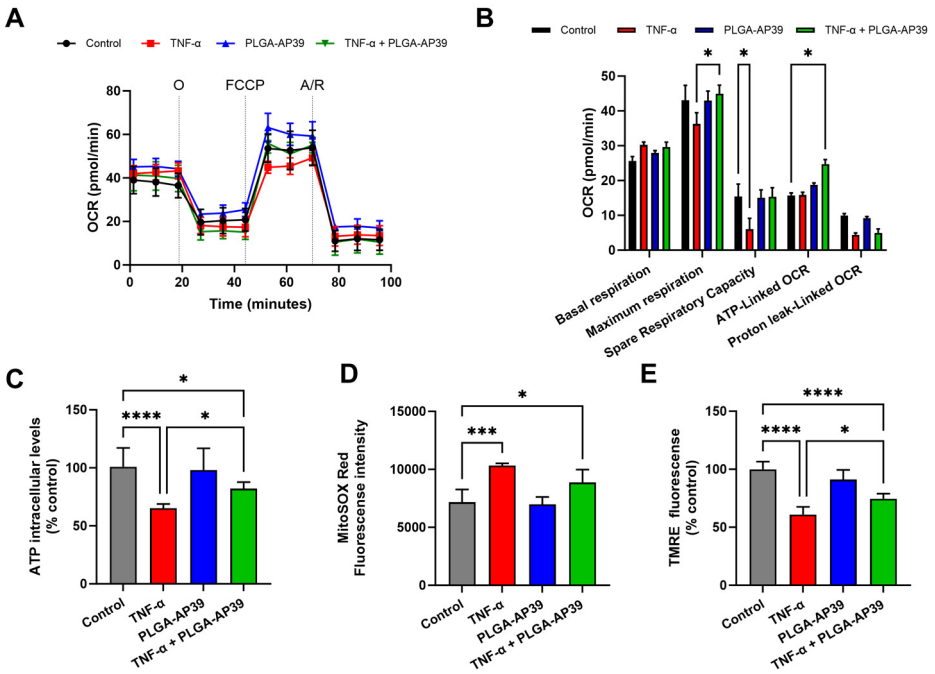

Figure 5. TNF-α-mediated mitochondrial dysfunction is partially ameliorated by AP39 delivered in novel PLGA NPs. (**A**) Oxygen consumption rates (OCR) were determined in real-time in HUVEC exposed to TNF-α (10 ng/mL) and or TNF-α (10 ng/mL) in combination with PLGA-AP39 diluted in media to final concentration of 0.3 μM followed by sequential injections of oligomycin (O), carbonyl cyanide 4-(trifluoromethoxy) phenylhydrazone (FCCP) and mixture of antimycin A and rotenone (A/R). (**B**) Parameters of mitochondrial function: basal respiration, maximal respiration, spare respiratory capacity, ATP-linked OCR and proton leak-linked OCR were calculated from OCR levels determined in (**A**). (**C**) Intracellular levels of ATP, (**D**) mitochondrial-specific ROS and (**E**) ΔΨm. Results are expressed as mean ± SD and analysed by one-way ANOVA followed by Tukey's multiple comparisons post hoc test to assess direct differences between individual groups. ($n = 3$). * $p \leq 0.05$, *** $p \leq 0.001$, and **** $p \leq 0.0001$.

Subsequently, we evaluated ATP levels as well as mitochondrial-specific ROS and ΔΨm as indicative of mitochondrial dysfunction. ATP levels were significantly reduced in the presence of TNF-α alone ($p < 0.001$ vs. control). However, we still observed that TNF-α in co-treatment with PLGA-AP39 displayed a statistically significant difference when compared to control ($p < 0.05$) (Figure 5C). A similar observation was perceived when assessing mitochondrial-specific ROS (Figure 5D). TNF-α alone significantly increased mitochondrial ROS ($p < 0.001$ vs. control). Finally, we assessed ΔΨm using the fluorescent probe, TMRE. Our results indicate that TNF-α depolarises the mitochondrial membrane potential (Figure 5E). Changes in ΔΨm are associated with mitochondrial dysfunction and induction of apoptotic cascade. Although statistically significant differences were still observed when TNF-α was co-administered with AP39-PLGA NPs, these results suggest that AP39 could partially prevent apoptosis and further cells' death under inflammatory environments.

3.6. PLGA-AP39 Ameliorate Vascular Dysfunction Associated with Inflammation

Our previous results suggest that mitochondrial dysfunction is partially restored in the presence of AP39 under inflammation caused by TNF-α. Our next approach was to investigate whether this partial restoration would improve endothelial cell function by assessing angiogenesis and would healing properties mediated by AP39. Angiogenesis was assessed by measuring branching parameters established in capillary-like structures formed by HUVEC cultured in the presence of TNF-α and PLGA-AP39 alone or in combination. Total branching length, total tube length and total segment length were significantly reduced in the presence of TNF-α alone while co-administration of TNF-α and PLGA-AP39 significantly improved total tube length ($p < 0.01$ vs. TNF-α). Interestingly, we observed that AP39-PLGA NPs alone moderately reduce total branching length and total segment length. These findings suggest that AP39 acts as a stress-responsive mitochondrial modulator rather than a constitutive enhancer of endothelial function (Figure 6). Moreover, we observed that wound closure was significantly improved when TNF-α was co-administered with AP39 delivered in PGA-NPs ($p < 0.01$ vs. TNF-α) (Figure 7). These results suggest that AP39 is able to improve vascular health in an inflammatory-prove environment established by TNF-α, suggesting a novel therapeutic avenue to improve vascular health in patients affected by vascular disorders associated with inflammation.

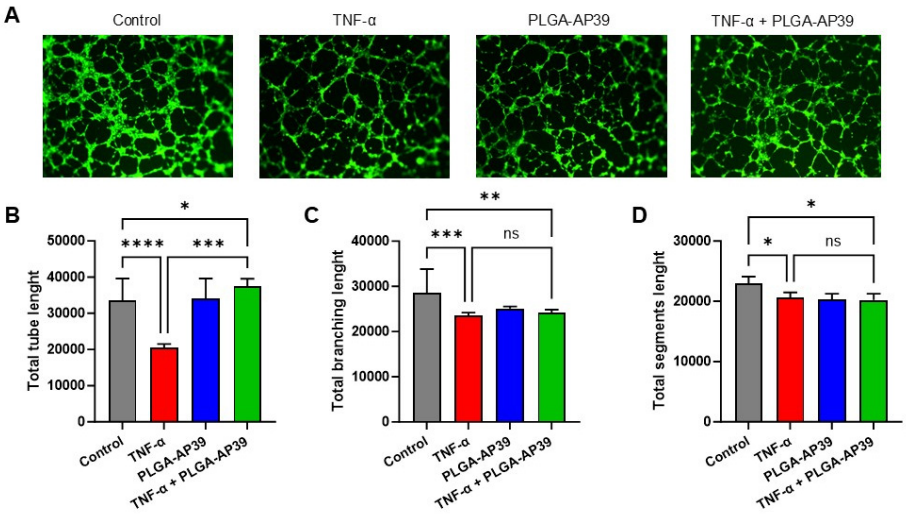

Figure 6. PLGA-AP39 partially restores capillary-like tube formation in HUVEC exposed to TNF-α. (**A**) Representative images of tube formation assay (×10 objective). (**B**) Total tube length, (**C**) total branching length and (**D**) total segment length. Results are expressed as mean ± SD and analysed by one-way ANOVA. ($n = 3$). * $p \leq 0.05$, ** $p \leq 0.01$, *** $p \leq 0.001$, and **** $p \leq 0.0001$.

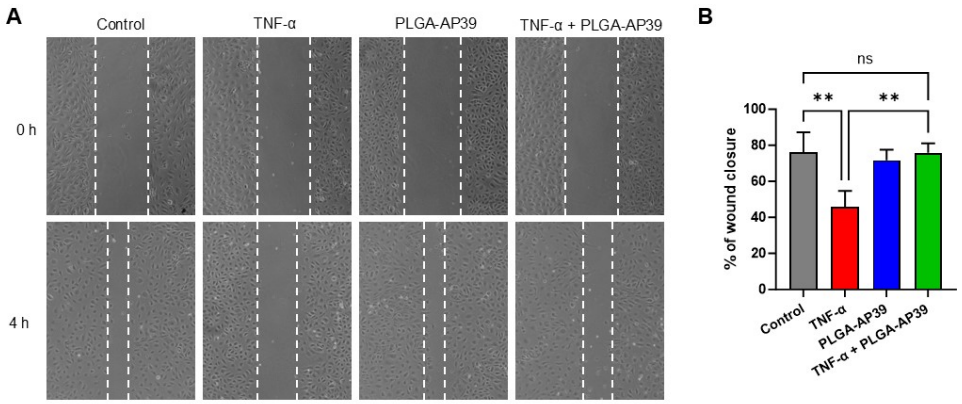

Figure 7. PLGA-AP39 restores endothelial cell migration in HUVEC exposed to TNF-α. (**A**) Representative images of time 0 h (scratch generated) and 4 h (after wound closure) of HUVEC exposed to TNF-α (10 ng/mL) or in combination with PLGA-AP39 (0.3 μM) (×10 objective). (**B**) Endothelial migration calculated as percentage of wound closure compared to time 0 h. Results are expressed as mean ± SD and analysed by one-way ANOVA. (n = 3). ** $p \leq 0.01$.

4. Discussion

In this study, we successfully fabricated and characterised PLGA NPs encapsulating AP39 (PLGA-AP39) and demonstrated their suitability as a potential intervention for inflammatory vascular disorders. To our knowledge, this is the first report describing the use of PLGA NPs for the targeted delivery of the mitochondria-directed H_2S donor, AP39, to counteract TNF-α-induced endothelial inflammation. The data presented here provide robust evidence of the anti-inflammatory and bioenergetic benefits of PLGA-AP39 in relevant vascular inflammation models. This strategy builds on extensive research within our group and the wider field, recognising the limitations of conventional H_2S donors, particularly their short half-life, which have hindered clinical translation [20]. PLGA-AP39 is an innovative approach able to enhance AP39's therapeutic delivery, prolong its bioavailability, and enable controlled release, thereby offering compelling new evidence to support the development of mitochondria-targeted H_2S therapies for conditions associated with chronic vascular inflammation, including diabetes and atherosclerosis.

Characterisation of our PLGA-AP39 provided evidence of a stable and scalable formulation approach. A mean particle size of approximately 226.9 ± 6.0 nm and a low polydispersity index of 0.195 ± 0.039 are consistent with a uniform dispersal, crucial for predictable biodistribution and enhanced bioavailability when used in vivo [30]. The defined size observed was within the nano range, and therefore these results are consistent with the previous literature suggesting that due to the identified size, our PLGA NPs are expected to carry payloads effectively while being able to penetrate the endothelium for effective intracellular targeting [22]. Size distribution is an important parameter for consideration in further translational and clinical development; therefore, future work would further require optimisation before in vivo or clinical translation studies begin. Additionally, zeta potential of +7 mV suggests that these NPs will maintain moderate stability in suspension, which is vital for their performance in biological environments. Moreover, we observed an encapsulation efficiency of 78.2%. Our lab previously demonstrated encapsulation efficiencies for other H_2S donors ranging from 65 to 85% [23]. Moreover, other authors have shown variable encapsulation efficiencies for hydrophobic molecules with values of approximately 67% in similar sized PLGA NPs (~193 nm) [22]. Therefore, an encapsulation of 78.2% suggests that our loaded method is effective. Taken together, the size and encapsulation efficiency observed suggests the suitability of PLGA as a viable vehicle for sustained drug release allowing higher capacity for encapsulation of the payload [22].

The release kinetics of AP39 from the PLGA NPs exhibited a controlled, sustained release profile when compared with the rapid release observed for AP39 in solution. This behaviour aligns with the purpose of utilising PLGA NPs for prolonged therapeutic activity, which is particularly advantageous in clinical applications where steady drug levels are required to exert therapeutic effects without toxicity [30]. Such controlled kinetics are vital for maintaining therapeutic drug concentrations within a safe and effective window [30], especially for gaseous mediators like H_2S that are otherwise rapidly cleared in vivo. The cumulative release data observed over seven days showed that PLGA-AP39 transitioned from an initial rapid release phase (as observed with AP39 in solution) to a slower, sustained phase. Our observations are consistent with our previous efforts to improve the release of the active metabolite, H_2S, when employing H_2S donors, ADTOH and sodium thiosulphate [12,23]. We have previously shown that PLGA NPs sustain the release of H_2S from sodium thiosulphate [23] while liposome encapsulation of AP39 delayed the release of both AP39 and H_2S [12]. This controlled release can potentially minimise side effects while maintaining efficacy, a principle that is especially relevant in treating chronic inflammatory conditions [30]. Moreover, given the fact that H_2S can exert biphasic effects on cellular health, particularly by disrupting the mitochondrial function at level of complex IV when in high concentration [31], our work here offers a solution to constrains in the translation of H_2S donors, such as AP39, to the clinic. Using PLGA NPs for the delivery of AP39 and thus H_2S might lead to reduced dosing frequency and minimised systemic side effects when used to treat human conditions.

The biological implications of our findings were investigated through the assessment of vascular inflammation responses mediated by TNF-α in endothelial cells. Induction of an inflammatory environment by TNF-α is a well-characterised method for pro-inflammatory cytokine production, serving as a suitable in vitro model to investigate inflammatory pathways and therapeutics [32]. Our results demonstrate that PLGA-AP39 successfully attenuated TNF-α-induced secretion of pro-inflammatory cytokines, including IL-6, IL-8, and TGF-β, suggesting that the anti-inflammatory properties of AP39 were preserved despite their encapsulation in PLGA and sustained due to the controlled release properties observed. These results are consistent with our previous reports on sodium thiosulphate mediated pro-angiogenic effects when delivered in PLGA NPs [23]. Moreover, other groups have shown the potential of H_2S donors to attenuate inflammation [33–38]. Although these investigations were carried out using H_2S donors not encapsulated into NPs, our observations are consistent with this extensive literature highlighting the anti-inflammatory properties of H_2S donors. This evidence supports the notion that the PLGA platform not only serves as a functional drug delivery system but also effectively preserves the pharmacological activity of AP39 against inflammation, which could provide a significant therapeutic advantage in the management of vascular diseases exacerbated by inflammatory processes, including conditions such as diabetes and atherosclerosis.

Mechanistically, our exploration into the effects of AP39 on mitochondrial bioenergetics suggests an enhancement in respiratory function when delivered in the PLGA format. Observations of improved maximum respiration rates and spare respiratory capacity when using PLGA NPs highlight the potential metabolic benefits of AP39 that are crucial in mitigating the bioenergetic impairments often seen in inflammatory states [11]. Our results here are consistent with our previous work on AP39 where we confirmed the bioenergetic protection that AP39 provides to mitochondria due to its ROS quenching properties, similar to observations reported elsewhere, and investigated under inflammatory-prone environments [11,14,39]. PLGA-AP39 increased ATP generation, mitigated mitochondrial ROS generation and modulated the $\Delta\Psi m$. These effects have been previously reported [11,14] and in this study, we were able to confirm that encapsulation in PLGA NPs retains the

antioxidant properties provided by AP39, suggesting its bioavailability and efficacy remain unaltered when delivered in these NPs. Together, these observations suggest that mitochondria-targeted delivery of AP39 does not merely mitigate inflammatory pathways but actively reprograms cellular bioenergetics towards a more homeostatic state. These observations hold particular promise for diseases where metabolic dysfunction and oxidative stress are central drivers of pathology, beyond chronic vascular inflammation.

Consistent with endothelial dysfunction, exposure to TNF-α alone significantly reduced total branching length, total tube length, and total segment length in HUVEC-derived capillary-like networks. Notably, co-administration of TNF-α and PLGA-AP39 significantly improved total tube length compared with TNF-α alone, indicating partial restoration of angiogenic competence under inflammatory conditions. In contrast, treatment with PLGA-AP39 alone resulted in a modest reduction in total branching length and total segment length under basal conditions. These findings underscore the context-dependent nature of mitochondria-targeted H_2S delivery. Rather than acting as a constitutive pro-angiogenic stimulus, AP39 appears to function as a stress-responsive mitochondrial modulator that preserves endothelial functional capacity under inflammatory conditions. Despite these encouraging findings, several limitations should be acknowledged. First, this study was conducted in vitro, using a well-established human endothelial cell line under a controlled inflammatory stimulus. While these models offer critical mechanistic insights, they cannot fully replicate the complexity of vascular inflammation in vivo, where multiple cell types, hemodynamic forces, and immune interactions contribute to disease progression. Moreover, although our results strongly suggest that AP39 exerts protective effects via mitochondrial pathways, further mechanistic studies are necessary to attribute AP39 an anti-inflammatory role, including mediated roles of the Nrf2 antioxidant response [18], S-sulfhydration of endothelial nitric oxide synthase (eNOS) [16], and NF-κB inhibition [19]. Nonetheless, establishing these molecular mechanisms was beyond the scope of our study. Therefore, further in vivo studies would validate the therapeutic promise of PLGA-AP39 in relevant animal models of vascular inflammation and endothelial dysfunction where an assessment of pharmacokinetics, biodistribution, mitochondrial targeting efficiency, and the impact on vascular integrity under pathological conditions such as diabetes and atherosclerosis would consolidate AP39 as an emerging therapeutic strategy to resolve inflammation.

Our findings open avenues for advanced nanomedicine solutions that combine organelle-specific targeting with controlled release employing polymeric nanocarriers and their use in the management of vascular and metabolic diseases where inflammation and mitochondrial dysfunction converge.

5. Conclusions

PLGA-AP39 nanoparticles are a novel strategy for resolving endothelial inflammation through targeted modulation of mitochondrial bioenergetics in a platform that offers controlled release while maintains targeting properties of AP39. This study provides foundational evidence for mitochondrial drug delivery using PLGA NPs and showcases its potential for resolving inflammatory vascular pathologies. PLGA-AP39 addressed key limitations associated with the short half-life and rapid clearance of conventional H_2S donors. Our findings highlight the therapeutic potential of combining advanced polymeric nanocarriers with organelle-targeted gasotransmitters to modulate vascular inflammation at its metabolic roots. Together, this work provides a strong proof of concept for a sustained, mitochondria-directed strategy to improve endothelial resilience and vascular health, setting the foundation for translational applications for AP39 as a mediator of chronic vascular inflammation disorders, including diabetes and atherosclerosis.

Supplementary Materials: The following supporting information can be downloaded at: https://www.mdpi.com/article/10.3390/clinbioenerg2010004/s1, Figure S1: Diagram representing oxygen consumption rates (OCR) measured in real-time using a Seahorse XFe24 Analyser. Sequential injections of drugs/modulators: oligomycin, (O) (1 μM), carbonyl cyanide 4-(trifluoromethoxy) phenylhydrazone (FCCP) (0.5 μM) and a mixture of rotenone and antimycin A (A/R) (1 μM) systematically modulate mitochondrial function by inhibiting complex V (ATP-synthase), depolarising the mitochondrial membrane and inhibiting complex I and III in mitochondria, respectively. The diagram illustrates calculations of parameters: basal and maximum respiration, spare respiratory capacity, ATP-linked respiration and non-mitochondrial respiration.; Figure S2: IL-10 levels in HUVEC exposed to TNF-α and PLGA-AP39. IL-10 levels were measured in cell culture media after exposure to TNF-α (10 ng/mL) or co-treated with TNF-α and PLGA-AP39 diluted in media to final concentration of 0.3 μM.

Author Contributions: Conceptualization, L.S.-A.; Methodology, L.S.-A., H.S., M.K.M.; Formal Analysis, L.S.-A., B.H.M., M.A.A.T., K.K., J.B., H.S., M.K.M.; Investigation, L.S.-A., B.H.M., M.A.A.T., K.K., J.B.; Resources, L.S.-A.; Data Curation, L.S.-A., M.A.A.T., M.K.M.; Writing—Original Draft Preparation, L.S.-A., M.K.M.; Writing—Review and Editing, L.S.-A., M.A.A.T., H.S., M.K.M.; Visualisation, L.S.-A.; Supervision, L.S.-A.; Project Administration, L.S.-A.; Funding Acquisition, L.S.-A. All authors have read and agreed to the published version of the manuscript.

Funding: This work was supported by the Royal Society Grant-Round 1 2021 (RGS/R1/221169) awarded to L.S.-A.

Data Availability Statement: Dataset available on request from the authors.

Acknowledgments: Diagram figures created in BioRender. Marwah, M. (2026) https://BioRender.com/xjpae51 (accessed on 11 February 2026).

Conflicts of Interest: The authors declare no conflicts of interest.

Abbreviations

A/R	Mixture of rotenone and antimycin A
ADTOH	5-(4-hydroxyphenyl)-3H-1,2- dithiole-3-thione
EGM-2	Endothelial Cell Growth Medium-2
eNOS	Endothelial nitric oxide synthase
ESEM	Environmental scanning electron microscopy
FCCP	Carbonyl cyanide 4-(trifluoromethoxy) phenylhydrazone
HPLC-UV	High-performance liquid chromatography with ultraviolet detection
HUVEC	Human umbilical vein endothelial cells
Hydrogen sulphide	H_2S
Na_2S	Sodium sulphide
NO	Nitric oxide
NPs	Nanoparticles
O	Oligomycin
OCR	Oxygen consumption rates
PBS	Phosphate-buffered saline
PDI	Polydispersity index
PLGA	Poly(lactic-co-glycolic acid)
PVA	Polyvinyl alcohol
ROS	Reactive oxygen species
SD	Standard deviation
STEM	Scanning transmission electron microscopy
TMRE	Tetramethylrhodamine ethyl ester
TNF-α	Tumour necrosis factor alpha
TPP+	Triphenylphosphonium
Ψm	Mitochondrial membrane potential

References

1. Wang, L.; Cheng, C.K.; Yi, M.; Lui, K.O.; Huang, Y. Targeting endothelial dysfunction and inflammation. *J. Mol. Cell. Cardiol.* **2022**, *168*, 58–67. [CrossRef]
2. Shaito, A.; Aramouni, K.; Assaf, R.; Parenti, A.; Orekhov, A.; Yazbi, A.E.; Pintus, G.; Eid, A.H. Oxidative Stress-Induced Endothelial Dysfunction in Cardiovascular Diseases. *Front. Biosci. (Landmark Ed.)* **2022**, *27*, 105. [CrossRef]
3. Marogianni, C.; Sokratous, M.; Dardiotis, E.; Hadjigeorgiou, G.M.; Bogdanos, D.; Xiromerisiou, G. Neurodegeneration and Inflammation—An Interesting Interplay in Parkinson's Disease. *Int. J. Mol. Sci.* **2020**, *21*, 8421. [CrossRef] [PubMed]
4. Totoń-Żurańska, J.; Mikolajczyk, T.P.; Saju, B.; Guzik, T.J. Vascular remodelling in cardiovascular diseases: Hypertension, oxidation, and inflammation. *Clin. Sci.* **2024**, *138*, 817–850. [CrossRef]
5. Sanchez-Aranguren, L.C.; Ahmad, S.; Dias, I.H.K.; Alzahrani, F.A.; Rezai, H.; Wang, K.; Ahmed, A. Bioenergetic effects of hydrogen sulfide suppress soluble Flt-1 and soluble endoglin in cystathionine gamma-lyase compromised endothelial cells. *Sci. Rep.* **2020**, *10*, 15810. [CrossRef]
6. Incalza, M.A.; D'Oria, R.; Natalicchio, A.; Perrini, S.; Laviola, L.; Giorgino, F. Oxidative stress and reactive oxygen species in endothelial dysfunction associated with cardiovascular and metabolic diseases. *Vasc. Pharmacol.* **2018**, *100*, 1–19. [CrossRef] [PubMed]
7. Kong, H.; Reczek, C.R.; McElroy, G.S.; Steinert, E.M.; Wang, T.; Sabatini, D.M.; Chandel, N.S. Metabolic determinants of cellular fitness dependent on mitochondrial reactive oxygen species. *Sci. Adv.* **2020**, *6*, eabb7272. [CrossRef]
8. Xiao, Q.; Ying, J.; Xiang, L.; Zhang, C. The biologic effect of hydrogen sulfide and its function in various diseases. *Medicine* **2018**, *97*, e13065. [CrossRef] [PubMed]
9. Cirino, G.; Szabo, C.; Papapetropoulos, A. Physiological roles of hydrogen sulfide in mammalian cells, tissues, and organs. *Physiol. Rev.* **2023**, *103*, 31–276. [CrossRef]
10. Lv, B.; Chen, S.; Tang, C.; Jin, H.; Du, J.; Huang, Y. Hydrogen sulfide and vascular regulation—An update. *J. Adv. Res.* **2021**, *27*, 85–97. [CrossRef]
11. Gerő, D.; Torregrossa, R.; Perry, A.; Waters, A.; Le-Trionnaire, S.; Whatmore, J.L.; Wood, M.; Whiteman, M. The novel mitochondria-targeted hydrogen sulfide (H(2)S) donors AP123 and AP39 protect against hyperglycemic injury in microvascular endothelial cells in vitro. *Pharmacol. Res.* **2016**, *113*, 186–198. [CrossRef]
12. Al Tahan, M.A.; Marwah, M.K.; Dhaliwal, M.; Diaz Sanchez, L.; Shokr, H.; Kaur, M.; Ahmad, S.; Badhan, R.K.S.; Dias, I.H.K.; Sanchez-Aranguren, L. Novel AP39-Loaded Liposomes Sustain the Release of Hydrogen Sulphide, Enhance Blood-Brain Barrier Permeation, and Abrogate Oxidative Stress-Induced Mitochondrial Dysfunction in Brain Cells. *Drug Des. Dev. Ther.* **2025**, *19*, 2067–2079. [CrossRef]
13. Marwah, M.K.; Manhoosh, B.; Shokr, H.; Al Tahan, M.A.; Stewart, R.; Iqbal, M.; Sanchez, L.D.; Abdullah, S.; Ahmad, S.; Wang, K.; et al. Transdermal delivery of mitochondrial-targeted hydrogen sulphide donor, AP39 protects against 6-hydroxydopamine-induced mitochondrial dysfunction. *Eur. J. Pharm. Biopharm.* **2023**, *191*, 166–174. [CrossRef]
14. Sanchez-Aranguren, L.; Marwah, M.K.; Nadeem, S. Neuroprotective effects of mitochondrial-targeted hydrogen sulphide donor, AP39 on H_2O_2-induced oxidative stress in human neuroblastoma SHSY5Y cell line. *Adv. Redox Res.* **2021**, *3*, 100024. [CrossRef]
15. Zhao, Y.; Wang, Y.; Zheng, H.; Xu, Q.; Zhou, K.; Liu, H.; Xia, Y.; Wei, D.H.; Jiang, M.; Tang, Z.H.; et al. Hydrogen sulfide upregulates SIRT1 to inhibit ox-HDL-induced endothelial cell damage and mitochondrial dysfunction. *Nitric Oxide* **2024**, *152*, 78–89. [CrossRef]
16. Altaany, Z.; Ju, Y.; Yang, G.; Wang, R. The coordination of S-sulfhydration, S-nitrosylation, and phosphorylation of endothelial nitric oxide synthase by hydrogen sulfide. *Sci. Signal.* **2014**, *7*, ra87. [CrossRef]
17. Stachowicz, A.; Wiśniewska, A.; Czepiel, K.; Pomierny, B.; Skórkowska, A.; Kuśnierz-Cabala, B.; Surmiak, M.; Kuś, K.; Wood, M.E.; Torregrossa, R.; et al. Mitochondria-targeted hydrogen sulfide donor reduces atherogenesis by changing macrophage phenotypes and increasing UCP1 expression in vascular smooth muscle cells. *Biomed. Pharmacother.* **2024**, *180*, 117527. [CrossRef]
18. Yang, G.; Zhao, K.; Ju, Y.; Mani, S.; Cao, Q.; Puukila, S.; Khaper, N.; Wu, L.; Wang, R. Hydrogen sulfide protects against cellular senescence via S-sulfhydration of Keap1 and activation of Nrf2. *Antioxid. Redox Signal.* **2013**, *18*, 1906–1919. [CrossRef]
19. Li, L.; Rose, P.; Moore, P.K. Hydrogen sulfide and cell signaling. *Annu. Rev. Pharmacol. Toxicol.* **2011**, *51*, 169–187. [CrossRef] [PubMed]
20. Sharif, A.H.; Iqbal, M.; Manhoosh, B.; Gholampoor, N.; Ma, D.; Marwah, M.; Sanchez-Aranguren, L. Hydrogen Sulphide-Based Therapeutics for Neurological Conditions: Perspectives and Challenges. *Neurochem. Res.* **2023**, *48*, 1981–1996. [CrossRef] [PubMed]
21. Kumari, A.; Yadav, S.K.; Yadav, S.C. Biodegradable polymeric nanoparticles based drug delivery systems. *Colloids Surf. B Biointerfaces* **2010**, *75*, 1–18. [CrossRef]
22. Palma-Chavez, J.A.; Fuentes, K.; Applegate, B.E.; Jo, J.A.; Charoenphol, P. Development and Characterization of PLGA-Based Multistage Delivery System for Enhanced Payload Delivery to Targeted Vascular Endothelium. *Macromol. Biosci.* **2021**, *21*, e2000377. [CrossRef]

23. Marwah, M.K.; Shehzad, S.; Shokr, H.; Sacharczuk, J.; Wang, K.; Ahmad, S.; Sanchez-Aranguren, L. Novel controlled-release polylactic-co-glycolic acid (PLGA) nanoparticles for sodium thiosulphate, a hydrogen sulphide donor, retains pro-angiogenic potential of hydrogen sulphide. *J. Exp. Nanosci.* **2022**, *17*, 197–213. [CrossRef]
24. Szczesny, B.; Módis, K.; Yanagi, K.; Coletta, C.; Le Trionnaire, S.; Perry, A.; Wood, M.E.; Whiteman, M.; Szabo, C. AP39, a novel mitochondria-targeted hydrogen sulfide donor, stimulates cellular bioenergetics, exerts cytoprotective effects and protects against the loss of mitochondrial DNA integrity in oxidatively stressed endothelial cells in vitro. *Nitric Oxide* **2014**, *41*, 120–130. [CrossRef]
25. Dranka, B.P.; Benavides, G.A.; Diers, A.R.; Giordano, S.; Zelickson, B.R.; Reily, C.; Zou, L.; Chatham, J.C.; Hill, B.G.; Zhang, J.; et al. Assessing bioenergetic function in response to oxidative stress by metabolic profiling. *Free Radic. Biol. Med.* **2011**, *51*, 1621–1635. [CrossRef] [PubMed]
26. Chung, C.Y.; Duchen, M.R. A Plate Reader-Based Measurement of the Cellular ROS Production Using Dihydroethidium and MitoSOX. *Methods Mol. Biol.* **2022**, *2497*, 333–337. [CrossRef] [PubMed]
27. Luna, C.; Carmona, A.; Alique, M.; Carracedo, J.; Ramirez, R. TNFα-Damaged-HUVECs Microparticles Modify Endothelial Progenitor Cell Functional Activity. *Front. Physiol.* **2015**, *6*, 395. [CrossRef]
28. Khan, S.; Awad, E.; Oszwald, A.; Mayr, M.; Yin, X.; Waltenberger, B.; Stupper, H.; Lipovac, M.; Uhrin, P.; Breuss, J. Premature senescence of endothelial cells upon chronic exposure to TNFα can be prevented by N-acetyl cysteine and plumericin. *Sci. Rep.* **2017**, *7*, 39501. [CrossRef]
29. Shao, Y.; Cheng, Z.; Li, X.; Chernaya, V.; Wang, H.; Yang, X. Immunosuppressive/anti-inflammatory cytokines directly and indirectly inhibit endothelial dysfunction- a novel mechanism for maintaining vascular function. *J. Hematol. Oncol.* **2014**, *7*, 80. [CrossRef]
30. Hines, D.J.; Kaplan, D.L. Poly(lactic-Co-Glycolic) Acid-Controlled-Release Systems: Experimental and Modeling Insights. *Crit. Rev. Ther. Drug Carr. Syst.* **2013**, *30*, 257–276. [CrossRef] [PubMed]
31. Paul, B.D.; Snyder, S.H.; Kashfi, K. Effects of hydrogen sulfide on mitochondrial function and cellular bioenergetics. *Redox Biol.* **2021**, *38*, 101772. [CrossRef]
32. Makó, V.; Czúcz, J.; Weiszhár, Z.; Herczenik, E.; Matkó, J.; Prohászka, Z.; Cervenak, L. Proinflammatory activation pattern of human umbilical vein endothelial cells induced by IL-1β, TNF-α, and LPS. *Cytom. Part A* **2010**, *77A*, 962–970. [CrossRef] [PubMed]
33. Yang, Y.W.; Deng, N.H.; Tian, K.J.; Liu, L.S.; Wang, Z.; Wei, D.H.; Liu, H.T.; Jiang, Z.S. Development of hydrogen sulfide donors for anti-atherosclerosis therapeutics research: Challenges and future priorities. *Front. Cardiovasc. Med.* **2022**, *9*, 909178. [CrossRef] [PubMed]
34. Ciccone, V.; Piragine, E.; Gorica, E.; Citi, V.; Testai, L.; Pagnotta, E.; Matteo, R.; Pecchioni, N.; Montanaro, R.; Di Cesare Mannelli, L.; et al. Anti-Inflammatory Effect of the Natural H2S-Donor Erucin in Vascular Endothelium. *Int. J. Mol. Sci.* **2022**, *23*, 15593. [CrossRef] [PubMed]
35. Zanardo, R.C.; Brancaleone, V.; Distrutti, E.; Fiorucci, S.; Cirino, G.; Wallace, J.L. Hydrogen sulfide is an endogenous modulator of leukocyte-mediated inflammation. *FASEB J.* **2006**, *20*, 2118–2120. [CrossRef]
36. Diaz Sanchez, L.; Sanchez-Aranguren, L.; Wang, K.; Spickett, C.M.; Griffiths, H.R.; Dias, I.H.K. TNF-α-Mediated Endothelial Cell Apoptosis Is Rescued by Hydrogen Sulfide. *Antioxidants* **2023**, *12*, 734. [CrossRef]
37. Faller, S.; Hausler, F.; Goeft, A.; von Itter, M.-N.A.; Gyllenram, V.; Hoetzel, A.; Spassov, S.G. Hydrogen sulfide limits neutrophil transmigration, inflammation, and oxidative burst in lipopolysaccharide-induced acute lung injury. *Sci. Rep.* **2018**, *8*, 14676. [CrossRef]
38. Hu, H.J.; Jiang, Z.S.; Zhou, S.H.; Liu, Q.M. Hydrogen sulfide suppresses angiotensin II-stimulated endothelin-1 generation and subsequent cytotoxicity-induced endoplasmic reticulum stress in endothelial cells via NF-kappaB. *Mol. Med. Rep.* **2016**, *14*, 4729–4740. [CrossRef]
39. Huang, Q.; Sparatore, A.; Del Soldato, P.; Wu, L.; Desai, K. Hydrogen sulfide releasing aspirin, ACS14, attenuates high glucose-induced increased methylglyoxal and oxidative stress in cultured vascular smooth muscle cells. *PLoS ONE* **2014**, *9*, e97315. [CrossRef]